CrossMark

ORIGINAL PAPER

P-V-T behavior of FeO(OH) and MnO(OH)

Felix Wiethoff[1] · Klaus-Dieter Grevel[1,2] · Bernd Marler[1] · Julia Herrmann[2] ·
Juraj Majzlan[2] · Jens Kirste[3] · Christian Lathe[4]

Abstract The *P-V-T* behavior of FeO(OH) and MnO(OH) has been determined under high pressure and high temperature up to 7.5 GPa and 500 °C using a MAX 80 cubic anvil high-pressure apparatus. The samples, synthetic goethite, α-FeO(OH), respectively, a natural groutite/manganite, α-MnO(OH)/γ-MnO(OH), specimen were mixed with Vaseline to ensure hydrostatic pressure-transmitting conditions, and NaCl served as an internal standard for pressure calibration. Energy-dispersive diffraction patterns were collected at a fixed 2θ angle ($\theta \approx 4.52°$). At pressures > 7.1 GPa and temperatures > 310 °C, respectively, $P > 6.3$ GPa and $T > 350$ °C, the transformation goethite ↔ ε-FeO(OH) was observed. Between 400 and 450 °C, the sample dehydrated to magnetite due to the reducing conditions caused by the graphite-tube furnace. By fitting a Birch–Murnaghan equation of state to the data, the bulk modulus of goethite was determined as (112.26 ± 2.26) GPa, $(K' = 4)$, $V_{T,0} = (138.79 \pm 0.10)$ Å^3·exp $[\int(0.497 \pm 0.103) \times 10^{-4} \, dT]$, $(\partial K_T/\partial T)_P = (-0.033 \pm 0.020)$ GPa K^{-1}. For ε-FeO(OH), the values $K = (142.8 \pm 15.1)$ GPa, $V_0 = (66.18 \pm 0.16)$ Å^3, $(K' = 4)$, were obtained. Groutite and manganite are more compressible than their Fe analogues. K(groutite) = (84.0 ± 2.9) GPa, $V_0 = (139.92 \pm 0.13)$ Å^3, $(K' = 4)$. K(manganite) = (82.2 ± 3.0) GPa, $V_0 = (135.37 \pm 0.15)$ Å^3, $(K' = 4)$. Groutite disappeared at $P \approx 5.5$ GPa and $T = 300$ °C, only manganite remained. At $T > 400$ °C, the sample dehydrated first to Mn$_3$O$_4$ [II] and then to manganosite (MnO) again pointing to reducing conditions.

✉ Klaus-Dieter Grevel
Klaus-Dieter.Grevel@rub.de

1 Institut für Geologie, Mineralogie und Geophysik, Ruhr-Universität Bochum, 44780 Bochum, Germany

2 Institut für Geowissenschaften, Bereich Mineralogie, Friedrich-Schiller-Universität Jena, Carl-Zeiss-Promenade 10, 07745 Jena, Germany

3 Institut für Mineralogie, Kristallographie und Materialwissenschaft, Universität Leipzig, Scharnhorststraße 20, 04275 Leipzig, Germany

4 Helmholtz-Zentrum Potsdam-Deutsches GeoForschungsZentrum GFZ, Zentrum für Geologische Speicherung, Telegrafenberg, 14473 Potsdam, Germany

Introduction

Fe$_2$O$_3$ and FeO(OH) in their different polymorphs constitute the majority of crystalline ferric oxides and oxyhydroxides on Earth (Majzlan et al. 2003a). Whereas most polymorphs are only stable at ambient pressure, goethite (α-FeO(OH)) and its dehydration product hematite (α-Fe$_2$O$_3$) can be observed at elevated pressure as well (Voigt and Will 1981). Bendeliani et al. (1972) synthesized a high-pressure polymorph of FeO(OH) during the studies of phase relations in the system Fe$_2$O$_3$-H$_2$O at $P = 9$ GPa and $T = 400$ °C. They reported this new phase, ε-FeO(OH), to be isostructural with manganite, γ-MnO(OH). Chenavas et al. (1973) also synthesized ε-FeO(OH) hydrothermally at 8 GPa and 500 °C and manganite at the same pressure and $T = 600$ °C. They found ε-FeO(OH) to have the orthorhombic InO(OH) structure, whereas the manganite structure is only pseudo-orthorhombic; the angle β of the unit cell deviates slightly from 90°, and the structure is monoclinic.

The phase relations in the system Fe_2O_3-H_2O were investigated up to ca. 7.5 GPa and 500 °C (Voigt and Will 1981) or up to 625 °C (Baneyeva and Bendeliani 1973). Both groups agree that the phase transition α-FeO(OH) ↔ ε-FeO(OH) is nearly temperature independent but, according to Baneyeva and Bendeliani (1973), the invariant point of the phases hematite + H_2O, goethite, and ε-FeO(OH) is to be found at 450 °C and 5.6 GPa, whereas Voigt and Will (1981) located it at 485 °C and 7.33 GPa. Gleason et al. (2008) published pressure–temperature stability studies of FeO(OH) using in situ X-ray diffraction measurements in a diamond anvil cell. They roughly validate the reaction boundaries between goethite and hematite + water as well as between α-FeO(OH) and ε-FeO(OH) as reported by Voigt and Will (1981). For goethite, the bulk modulus $K = (140.3 \pm 3.7)$ GPa, $K' = 4.6 \pm 0.4$ was reported, for ε-FeO(OH), Gleason et al. (2008) obtained $K = (158 \pm 5)$ GPa with K' assumed to be 4 (Table 1). A few other studies of the high-pressure behavior of FeO(OH) can be found in the literature. They are also listed in Table 1. Kim and Yi (1997) obtained $K = 147.9$ GPa for goethite. This value is similar to the value of Gleason et al. (2008) but differs significantly from the bulk modulus reported by Nagai et al. (2003), $K = (111 \pm 2)$ GPa. Both groups assumed K' to be 4. Fernando et al. (2012) investigated the compressibility of nanoparticulate goethite and compared their results to the measurements of Nagai et al. (2003). According to their studies, the bulk modulus of nanoparticulate goethite, $K = (109.4 \pm 2.2)$ GPa, is very similar to that of bulk goethite. The high-pressure polymorph, ε-FeO(OH), was investigated by Suzuki et al. (2010). They found $K = (126 \pm 3)$ GPa and its pressure derivative $K' = 10 \pm 1$.

Much less is known about the behavior of MnO(OH) at elevated pressure and temperature. Although also synthesized at high pressure and temperature by Chenavas et al. (1973), manganite occurs in nature associated with other manganese oxides in deposits formed by circulating low-temperature hydrothermal fluids, commonly with a significant contribution of meteoric waters. Often it is formed in low-temperature hydrothermal veins in association with calcite, barite and siderite (Klein and Hurlbut 1993; Majzlan et al. 2016). Groutite (α-MnO(OH)), the Mn-analogue of goethite, was first described by Gruner (1947) from the Cuyuna range, Minnesota, associated with iron ores. Kohler et al. (1997) refined the crystal structures of groutite and manganite. They also investigated the behavior of both MnO(OH) polymorphs at elevated temperature by in situ temperature-dependent single-crystal X-ray diffraction and found that both phases transform in air above ca. 300 °C to β-MnO_2 (pyrolusite). The bulk modulus of manganite was reported recently to be (91 ± 3) GPa by Suzuki (2013). The compressibility of groutite and the P-V-T behavior of both minerals are not known.

There are still some discrepancies concerning the bulk moduli of the FeO(OH) polymorphs and the Fe_2O_3-H_2O phase diagram. In this study, we are addressing some of the inconsistencies by in situ powder X-ray diffraction (XRD) data of FeO(OH) using a MAX 80 cubic anvil high-pressure apparatus. Additionally, the P-V-T behavior of a natural groutite–manganite sample was investigated.

Samples

FeO(OH): The synthetic goethite sample prepared by Majzlan et al. (2003a) was used. The lattice parameters obtained by Majzlan et al. (2003a) are listed in Table 2.

MnO(OH): The groutite sample comes from the village Zaval'evka, south of the city Gajworon in the Kirovograd

Table 1 Compressibility data of goethite, ε-FeO(OH), groutite and manganite; literature values in comparison with this study

Phase	Bulk modulus K [GPa]	Pressure derivative K'	Volume at ambient pressure V_0 [Å³]	Technique	References
Synthetic goethite	109.4 ± 2.2	4	140.45	DAC	Fernando et al. (2012)
Synthetic goethite	111 ± 2	4	140.45 ± 1	DAC	Nagai et al. (2003)
Synthetic goethite	140.3 ± 3.7	4.6 ± 0.4	138.75 ± 0.02	DAC	Gleason et al. (2008)
Natural goethite	147.9	4	139.3	DAC	Kim and Yi (1997)
Synthetic goethite	112.3 ± 2.3	4	138.79 ± 0.10	Multi-anvil press	This study
ε-FeO(OH)	126 ± 3	10 ± 1	66.20 ± 0.03	Multi-anvil press	Suzuki (2010)
ε-FeO(OH)	158 ± 5	4	66.3 ± 0.5	DAC	Gleason et al. (2008)
ε-FeO(OH)	142.8 ± 15.1	4	66.18 ± 0.16	Multi-anvil press	This study
Natural manganite	91 ± 3	7 ± 1	270.47 ± 0.09^{a}	Multi-anvil press	Suzuki (2013)
Natural manganite	82.2 ± 3.0	4	135.37 ± 0.15	Multi-anvil press	This study
Natural groutite	84.0 ± 2.9	4	139.92 ± 0.13	Multi-anvil press	This study

DAC diamond anvil cell

[a] Spacegroup $B2_1/d$

Table 2 Lattice parameters of the studied phases

Phase	a (Å)	b (Å)	c (Å)	β (°)	V (Å³)	Spacegroup	References
Goethite, FeO(OH)	4.6089 ± 0.0003	9.9550 ± 0.0006	3.0224 ± 0.0002		138.67 ± 0.02	*Pbnm*	Majzlan et al. (2003a)
Groutite, MnO(OH)	10.667 ± 0.001	2.871 ± 0.001	4.554 ± 0.001		139.47 ± 0.06	*Pnma*	Kohler et al. (1997)
Groutite, MnO(OH)	10.6649 ± 0.0005	2.8718 ± 0.0001	4.5567 ± 0.0002		139.56 ± 0.01	*Pnma*	This study
Manganite, MnO(OH)	5.304 ± 0.001	5.277 ± 0.001	5.304 ± 0.001	114.38 ± 0.02	135.22 ± 0.05	*P2$_1$/c*	Kohler et al. (1997)
Manganite, MnO(OH)	5.3044 ± 0.0003	5.2739 ± 0.0003	5.3099 ± 0.0003	114.4784 ± 0.0003	135.20 ± 0.04	*P2$_1$/c*	This study

region, Ukraine. Black, spherical aggregates of MnO(OH) minerals grow on calcite; they contain mostly groutite, with about 20 wt% manganite. For the XRD experiments, the sample was finely ground. A Rietveld refinement of an XRD pattern obtained at a Bruker D8 diffractometer in Bochum yielded the lattice parameters listed in Table 2. The values are in good agreement with the data of Kohler et al. (1997).

Experimental

In situ XRD experiments were carried out using a MAX 80 cubic anvil high-pressure apparatus, which was installed at beamline F.2.1 of the DORIS III storage ring of HASYLAB (Desy, Hamburg, Germany). The experimental setup as described in detail by Grevel et al. (2000) and Darul et al. (2013) will be repeated here briefly.

A quasi-isostatic pressure environment was generated by six tungsten carbide anvils with 6×6 or 4×4 mm² square truncations in a cubic arrangement. In Fig. 1, the high-pressure boron–epoxy sample assembly is shown. Corresponding to the edge length of 8 or 6 mm, it contained a graphite-tube furnace with a diameter of 4 or 3 mm, respectively. This graphite resistance heater also acted as sample container for up to five different sample or standard layers. Due to problems during the sample preparation, we abstained from using an additional hexagonal boron nitride (hBN) capsule within the graphite heater (cf. Darul et al. 2013). The temperature was controlled by a Nicrosil–Nisil (type N) thermocouple within $\pm 2\,°C$; no correction was made for the effect of pressure on the thermocouple electromotive force (emf). The overall uncertainty in temperature due to possible temperature gradients in the high-pressure cell is estimated to be $\pm 30\,°C$. The powdered samples were mixed with Vaseline as a pressure medium to ensure hydrostatic pressure-transmitting conditions (cf. Grevel et al. 2000). Vaseline or petroleum jelly (CAS #: 8009-03-8) consists of saturated hydrocarbons with carbon numbers mainly higher
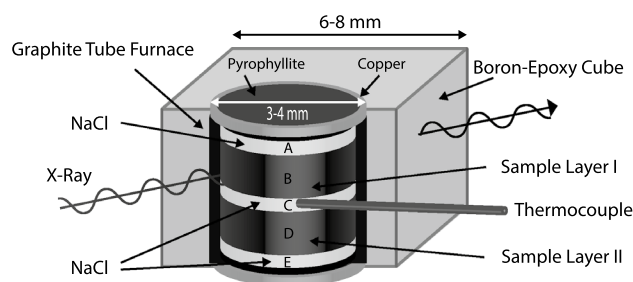

Fig. 1 Sketch of the high-pressure, high-temperature cell assembly. Heating is realized through a graphite resistance heater which also functions as sample container. The powdered samples (layers *B, D*) are mixed with Vaseline for hydrostatic pressure transmission, NaCl layers (marked *A, C, E*) act as pressure standard. Commonly, layer *C* (containing the thermocouple) was a NaCl/hBN mixture. Measurements correspond to large cubes (8/4 mm) or small cubes (6/3 mm), respectively. In our small cube experiments, only a single sample layer was investigated. The whole cell can be moved up- or downwards, thus positioning different layers into the X-ray beam path which is fixed

than 25. It is insoluble in water and not readily acted on by chemical reagents (cf. http://www.inchem.org/documents/icsc/icsc/eics1440.htm). Directly adjacent pellets of powdered NaCl served as a diffraction standard for pressure determination. The vertical pressure variation due to internal stress and small variations in pressure control (± 0.5 tons) between single layers of the standard (Fig. 1) was in the range 0.05–0.25 GPa; therefore, an overall uncertainty of ± 0.25 GPa was assumed during the evaluation of the data (see below).

A white synchrotron beam of 100×100 µm² dimension was used for carrying out the measurements. Energy-dispersive diffraction patterns were collected at a fixed 2θ angle ($\theta \approx 4.52°$), which was determined for each run from the diffraction pattern of NaCl at ambient conditions. Spectra were collected using a Canberra germanium solid-state detector with a resolution varying from 135 eV at 6.3 keV to 450 eV at 122 keV. By means of a peak-search program for the evaluation of Gauss-shaped diffraction patterns

(Lauterjung et al. 1985), peak positions were determined automatically after subtracting the background.

Two experimental runs using 8-mm cubes were carried out, run 5 contained FeO(OH) and MnO(OH), run 6 only MnO(OH) (Table S1a–c; online resource 1). Another five successful experiments were run using only goethite as starting material in 6-mm cubes. Usually, the samples were compressed in several steps to a selected pressure at room temperature and then heated until either a breakdown reaction occurred or the thermocouple showed fluctuations in temperature indicating problems with heating. In runs 25, 28 and 30 other *P-T* paths were chosen (cf. Table S1a, online resource 1). Diffraction data were collected for about three minutes. A subset of at least four of the NaCl diffraction maxima with Bragg indices 111, 200, 220, 311, 222, 400, 420 and 422 was used to calculate its cell parameter at different *P-T* conditions. Using this parameter and the measured temperature, pressure values were determined from the Decker equation of state (EOS) for NaCl (Decker 1971).

Goethite diffraction data were evaluated using the structural data given by Majzlan et al. (2003a). Indexing of ε-FeO(OH) followed Voigt and Will (1981) and Suzuki et al. (2010). Groutite and manganite were indexed based on Kohler et al. (1997).

Results and discussion

FeO(OH): phase diagram

In a pressure–temperature diagram (Fig. 2), all measured points and postulated phase boundaries from previous studies (Baneyeva and Bendeliani 1973; Voigt and Will 1981) are shown. The breakdown reaction of FeO(OH) could be observed around 400–450 °C (runs 5, 22, 28, 30; see Fig. 3a). At that temperature, the dehydration occurs, however, due to the reducing conditions caused by the graphite-tube furnace (cf. Fig. 1) and probably also by the Vaseline, FeO(OH) decomposed to Fe_3O_4 (magnetite) and H_2O and not to Fe_2O_3 (hematite) and H_2O, as expected. In the run 22 at 500 °C, even wüstite (FeO) could be detected. These observations confirm the dehydration boundary (2 FeO(OH) $\rightarrow$ $Fe_2O_3 + H_2O$) at non-reducing conditions reported by Voigt and Will (1981) within uncertainties.

The α→ε phase transition shown in Fig. 3b could be localized between 325 and 350 °C at 6.6 GPa (isobaric path, run 30) and between 6.2 and 6.6 GPa at 350 °C (isothermal path, run 28) (see Fig. 2, phase transition) and seems to be kinetically inhibited below 250 °C. The refinement of the unit-cell parameters of α-FeO(OH) and ε FeO(OH) related to the spectrum depicted in Fig. 3b is shown in Tables 3 and 4, respectively. We conclude that
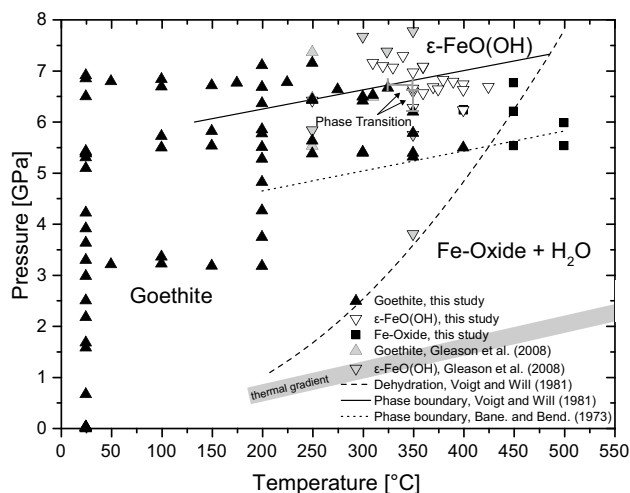

Fig. 2 Pressure–temperature diagram of the FeO(OH) system showing all measured points and postulated phase boundaries from previous studies. Due to the reducing conditions, FeO(OH) decomposed to $Fe_3O_4 + H_2O$. The α→ε phase transition highlighted by *arrows* could be localized between 325 and 350 °C at 6.6 GPa (isobaric path) and between 6.2 and 6.6 GPa at 350 °C (isothermal path). The *shaded gray line* illustrates a low geothermal gradient ($\approx 4.4°$ / km) under continental shields [after Jaupart and Mareschal (1999) and Winter (2014)] which is very similar to the cold Martian thermal gradient suggested by Verhoeven et al. (2005) and Zharkov and Gudkova (2014)

the nearly pressure-independent α-ε boundary is confirmed and the values of Voigt and Will (1981) are most appropriate. In two runs, the sample was cooled stepwise and finally depressurized to ambient pressure after the ε phase occurred. In contrast to Gleason et al. (2008), ε-FeO(OH) could be quenched to ambient conditions. The reverse reaction ε-FeO(OH) → goethite was not observed in our study.

FeO(OH): equation of state

Unit-cell volume and unit-cell parameters of the FeO(OH) polymorphs and their dehydration products as a function of pressure and temperature are listed in Table S1a (online resource 1).

By fitting a Birch–Murnaghan equation of state

$$P = 1.5 \times K_T \times \left[V_{T,r}^{-7} - V_{T,r}^{-5} \right] \times \left[1 - 0.75 \times \left(4 - K_T' \right) \times \left(V_{T,r}^{-2} - 1 \right) \right],$$

$$V_{T,r} \equiv \left(V/V_{T,0} \right)^{1/3}, \quad V_{T,0} = V_0 \exp \left(\int \alpha_{T,0} \mathrm{d}T \right)$$

(1)

to the data, the values of the isothermal bulk modulus, K, and its pressure derivative, K', can be derived. V is the unit-cell volume at high pressure P (in GPa) and temperature T (in K), and V_0 is the volume at ambient pressure. $K_T = K + (\partial K_T / \partial T)_P \times (T - T_0)$, K_T' and $V_{T,0}$ are the isothermal bulk modulus, its pressure derivative and the unit-cell volume
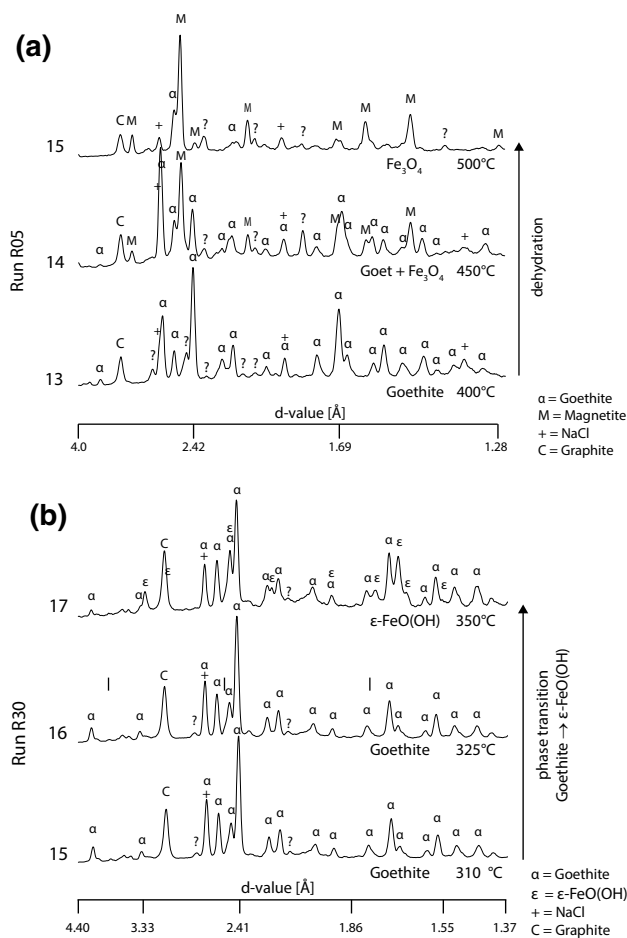
(a)

Run R05

15   Fe_3O_4 500 °C

14   Goet + Fe_3O_4 450 °C

13   Goethite   400 °C

dehydration

d-value [Å]

4.0   2.42   1.69   1.28

α = Goethite
M = Magnetite
+ = NaCl
C = Graphite

(b)

Run R30

17   ε-FeO(OH)   350 °C

16   Goethite   325 °C

15   Goethite   310 °C

phase transition
Goethite → ε-FeO(OH)

d-value [Å]

4.40   3.33   2.41   1.86   1.55   1.37

α = Goethite
ε = ε-FeO(OH)
+ = NaCl
C = Graphite

Fig. 3 **a** Dehydration of goethite to magnetite (run 5); **b** phase transition goethite → ε-FeO(OH) (run 30)

Table 3 Refinement of the unit-cell parameters of α-FeO(OH) (goethite), Run R30-17 (T = 350 °C, P = 6.66 GPa)

$h\,k\,l$	d_{obs}	d_{calc}	$d_{obs} - d_{calc}$
1 1 0	4.102	4.101	0.001
1 2 0	3.327	3.329	−0.003
1 3 0	2.661	2.659	0.002
0 2 1	2.563	2.563	0.000
1 1 1	2.422	2.420	0.001
1 2 1	2.231	2.228	0.003
1 4 0	2.165	2.165	0.000
2 1 1	1.771	1.772	−0.001
2 2 1	1.693	1.693	0.000
2 3 1	1.580	1.580	0.000
1 5 1	1.550	1.549	0.001
0 0 2	1.499	1.499	0.000
0 6 1	1.442	1.443	−0.001

Table 4 Refinement of the unit-cell parameters of ε-FeO(OH), Run R30-17 (T = 350 °C, P = 6.6 GPa)

$h\,k\,l$	d_{obs}	d_{calc}	$d_{obs} - d_{calc}$
1 1 0	3.267	3.259	0.008
0 1 1	2.467	2.466	0.001
1 1 1	2.202	2.204	−0.002
2 0 1	1.909	1.899	0.010
2 1 1	1.739	1.741	−0.002
1 2 1	1.662	1.657	0.005
2 2 0	1.633	1.630	0.003
3 1 0	1.532	1.534	−0.002
1 1 2	1.359	1.359	0.000
0 3 1	1.306	1.306	0.000
2 3 1	1.152	1.153	−0.001

$$\alpha_{T,0} = a + bT. \tag{2}$$

In Eqs. (1) and (2), V_0, K, K'_T, $(\partial K_T/\partial T)_P$, a and b are considered as fit parameters, which were obtained by fitting Eq. (1) to the experimental unweighted data of the respective phases (Table S1a, online resource 1). As indicated by the uncertainties after the first fit, the measured volumes scatter too much to obtain precise values of b and K'_T. Therefore, K'_T was kept constant at a value of 4 and b was omitted (i.e., b = 0) in all cases.

Accordingly, the bulk modulus of goethite was determined as K = (112.3 ± 2.3) GPa, $V_{T,0}$ (goethite) = (138.79 ± 0.10) Å³·exp [$\int$(0.497 ± 0.103)×10⁻⁴ dT], $(\partial K_T/\partial T)_P$ = (−0.033 ± 0.020) GPa K⁻¹. The unit-cell volume of goethite as a function of pressure at room temperature is depicted in Fig. 4 and the compressibility behavior of the cell parameters is shown in Fig. 5. Goethite deforms anisotropically; the a and c axes are more compressible than the b axis, a being the most compressible one. A similar compressibility behavior was observed for the isostructural Al-analogue diaspore (Grevel et al. 2000). Our K_T value is in good agreement with the values reported by Nagai et al. (2003) and Fernando et al. (2012) (Table 1). On the other hand, these authors both reported a much higher volume at zero pressure. Our data confirm a parallel shift of the EOS curve to smaller values of the unit-cell volume which is in accordance with the unit-cell data at ambient conditions (Majzlan et al. 2003a). Compressibility data by Kim and Yi (1997) and Gleason et al. (2008) deviate significantly from both lines probably due to non-hydrostaticity effects.

Gualtieri and Venturelli (1999) investigated the temperature-induced goethite-hematite phase transformation at ambient pressure by in situ synchrotron X-ray powder diffraction. They used the orthorhombic space group *Pnma* for goethite having a = 9.95 Å, b = 3.01 Å, c = 4.62 Å (Z = 4) because this unit cell could be easily compared to the one of hematite in which the c axis is coincident and three

at temperature T and 0.1 MPa, respectively, T_0 = 298.15 K. The thermal expansion at ambient pressure, $\alpha_{T,0}$, can be approximated as
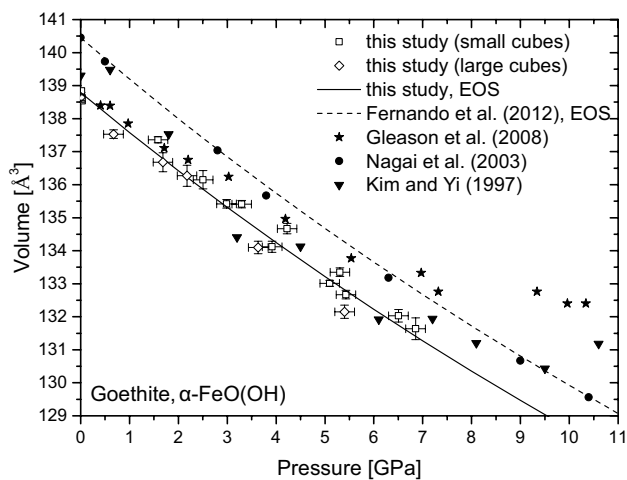
Fig. 4 Volume compressibility of goethite at room temperature in comparison with the literature values. Note the much higher volume at zero pressure reported by Nagai et al. (2003) and Fernando et al. (2012). Our data confirm a parallel shift of the EOS (*dashed line*) curve to smaller values of the unit-cell volume (*solid line*) which is in accordance with unit-cell literature data at ambient conditions (e.g., Majzlan et al. 2003a)
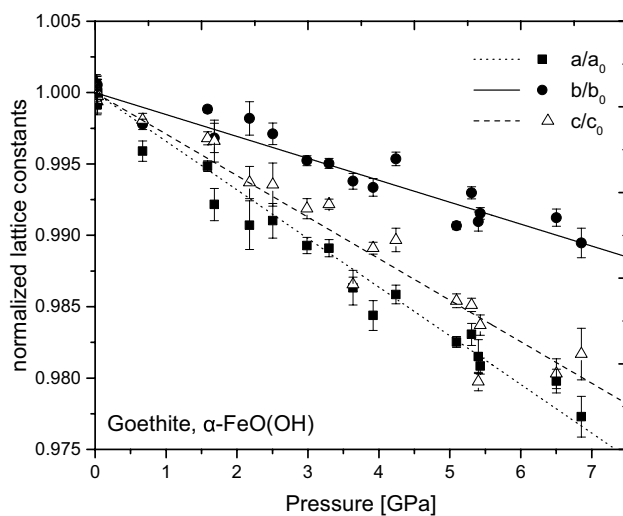

Fig. 5 Compressibility behavior of the cell parameters of goethite normalized to values from Majzlan et al. (2003a). Linear fits are shown to guide the eye

times the c axis of goethite. The decomposition of goethite started at about 200 °C. During the transformation, Gualtieri and Venturelli (1999) observed a dramatic decrease in the cell parameter b which determined a volume contraction of goethite while a and c expanded. Therefore, we checked our high-pressure goethite data at elevated temperature but perhaps due to the scatter of the data we did not observe a similar trend in the cell parameters. The scatter is also reflected by the large uncertainty in the thermal

expansion coefficient $\alpha = (0.497 \pm 0.103) \times 10^{-5}$ K^{-1} which thus should be used with some caution.

Our Birch–Murnaghan fitting procedure for the ε-FeO(OH) phase yielded: $K = (142.8 \pm 15.1)$ GPa, $V_0 = (66.18 \pm 0.16)$ Å^3, ($K' = 4$). This is in accordance with values from the literature (cf. Table 1).

MnO(OH): phase diagram

Since our natural sample contained both MnO(OH) polymorphs, groutite, α-MnO(OH) and manganite, γ-MnO(OH), we were able to investigate the behavior of both phases at high pressure and temperature. For the refinement procedure, only those reflections were used which clearly could be assigned to either groutite or manganite. Unit-cell volume and unit-cell parameters of groutite as a function of pressure and temperature are listed in Table S1b (online resource 1); the data for manganite can be found in Table S1c (online resource 1). While increasing the pressure, MnO(OH) diffraction patterns were obtained at two different positions in the sample layer (e.g., no. 4 and 4b in run 5 at $P = 2.18$ GPa). The differences in the lattice parameters may reflect some pressure gradient and also a different grade of sample homogeneity. Between $T = 250$ °C and $T = 300$ °C at $P \approx 5.5$ GPa groutite clearly disappeared, only the manganite reflections remained indicating a phase transition groutite → manganite (no. 10 and 11 in run 5, see Fig. 6a). The refinement of the unit-cell parameters of α-MnO(OH) and γ-FeO(OH) related to the spectrum depicted in Fig. 6a is shown in Tables 5 and 6, respectively.

Both groutite, α-MnO(OH) and manganite, γ-MnO(OH), transform in air above ca. 300 °C to β-MnO$_2$ (pyrolusite) (Kohler et al. 1997). In our experiments, we observed dehydration to manganosite (MnO) in both runs, probably again caused by the reducing conditions. In run 5–14 at $T = 450$ °C, manganite disappeared and several new reflections occurred pointing to an intermediate phase. This phase is still seen in run 5–15 ($T = 500$ °C) besides manganosite (see Fig. 6b), however, with less intense reflections.

In a HRTEM study of the transformation from manganite to pyrolusite, Rask and Buseck (1986) observed the phase Mn$_5$O$_8$ and also described another new Mn oxide. They suggested that this new phase is a structural modification of pyrolusite. Post and Heaney (2004) investigated the structures and dehydration behaviors of ramsdellite, MnO$_2$ and groutellite, ideally Mn$^{4+}_{0.5}$Mn$^{3+}_{0.5}$O$_{1.5}$(OH)$_{0.5}$, a phase that is generated synthetically as an intermediate compound during the reduction of ramsdellite to groutite (Klingsberg and Roy 1959). The latter authors also determined the univariant *P-T* curves for the reactions Mn(OH)$_2$ (pyrochroite) = MnO (manganosite) + H$_2$O and 2 γ-MnOOH (manganite) = Mn$_2$O$_3$ (bixbyite) + H$_2$O up to about 400 MPa. We compared the reflections of
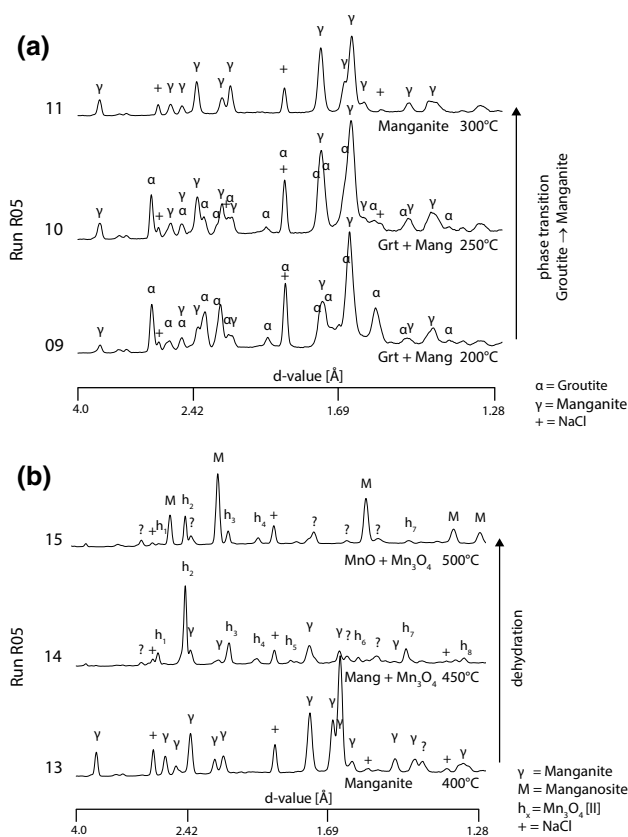
Fig. 6 **a** At $P \approx 5.5$ GPa and $T = 250\,^\circ$C, groutite clearly disappeared, and only the manganite reflections remained indicating a phase transition groutite → manganite (run 5). **b** Dehydration of manganite to manganosite, note the appearance of the marokite-like high-pressure polymorph of Mn_3O_4 (named Mn_3O_4 [II]) in run 5–14; the following reflections (denoted h_n) were assigned to Mn_3O_4 [II], listed are d-values [Å]: (1) 2.654—(320); (2) 2.432—(040); (3) 2.143—(131); (4) 2.008—(231); (5) 1.838—(411); (6) 1.588—(600); (7) 1.449—(351); (8) 1.309—(322); (9, not shown) 1.215—(080). The reflections (040) and (080) are very strong indicating preferred orientation

Table 5 Refinement of the unit-cell parameters of α-MnO(OH) (groutite), Run R05-10 ($T = 250\,^\circ$C, $P = 5.64$ GPa)

$h\,k\,l$	d_{obs}	d_{calc}	$d_{obs} - d_{calc}$
3 0 1	2.756	2.761	−0.005
4 0 0	2.620	2.628	−0.008
2 1 0	2.507	2.507	0.000
1 1 1	2.341	2.346	−0.005
4 0 1	2.262	2.267	−0.005
2 1 1	2.192	2.188	0.004
2 0 2	2.054	2.062	−0.008
3 1 1	1.988	1.984	0.004
4 1 0	1.939	1.933	0.006
5 0 1	1.902	1.904	−0.002
4 1 1	1.783	1.775	0.008
1 1 2	1.731	1.738	−0.007
4 0 2	1.698	1.706	−0.008
2 1 2	1.675	1.671	0.004
5 1 1	1.589	1.583	0.006
5 0 2	1.530	1.534	−0.004
6 1 0	1.490	1.493	−0.003
0 2 0	1.421	1.426	−0.005
3 0 3	1.377	1.375	0.002
3 2 1	1.268	1.267	0.001
6 1 2	1.245	1.243	0.002
8 0 2	1.133	1.134	−0.001
1 0 4	1.115	1.115	0.000

the intermediate phase (see Fig. 6b) to XRD patterns of groutellite, the phase Mn_5O_8, pyrochroite and several other Mn-hydroxides and -oxides, e.g., feitknechteite, β-MnO(OH), nsutite, γ-MnO_2 or more exactly $(Mn^{4+}, Mn^{2+})(O, OH)_2$, ramsdellite, pyrolusite, akhtenskite, ε-MnO_2 (Chukhrov et al. 1989; Chabre and Pannetier 1995), bixbyite, and hausmannite, Mn_3O_4, however, without a convincing match. Finally, we compared our diagram to the pattern obtained for a high-pressure polymorph of hausmannite. Hausmannite, a tetragonal substructure of the spinel structure, has been reported by Reid and Ringwood (1969) to transform at 12 GPa and 900 °C into an orthorhombic phase with marokite, $CaMn_2O_4$, structure (Ross et al. 1990). Paris et al. (1992) described the phase transition and the compressibility of both polymorphs in more detail. They designated Mn_3O_4 in the low-pressure hausmannite structure as Mn_3O_4 [I]

and the high-pressure marokite-like polymorph as Mn_3O_4 [II]. The behavior of Mn_3O_4 as a function of pressure and temperature was studied by in situ high-pressure high-temperature powder diffraction measurements recently (Darul et al. 2013). These experiments also were carried out at HASYLAB using the same experimental setup as described above. Upon heating the sample under the pressure of 7.20 GPa, Darul et al. (2013) observed the tetragonal-to-orthorhombic phase transition at $T \sim 400\,^\circ$C. Now, we were able to assign most of the formerly unknown reflections successfully (see Fig. 6b). At $P \sim 5.5$ GPa, manganite decomposed first to Mn_3O_4 [II] at $T \sim 450\,^\circ$C and then to manganosite (MnO) with increasing temperature. The cell parameters obtained for Mn_3O_4 [II] (Table S1c, online resource 1) are in a good agreement with the parameters reported by Paris et al. (1992) at room temperature.

Based on these observations, we propose a phase diagram of MnO(OH) (Fig. 7) similar to the diagram for FeO(OH) as shown in Fig. 2. It has to be noted again that dehydration of FeO(OH) and MnO(OH) took place under reducing conditions. Under air, MnO(OH) would probably decompose to bixbyite or pyrolusite. This has to be investigated in more detail in future.

Table 6 Refinement of the unit-cell parameters of γ-MnO(OH) (manganite), Run R5-10 ($T = 250\,°C$, $P = 5.64$ GPa)

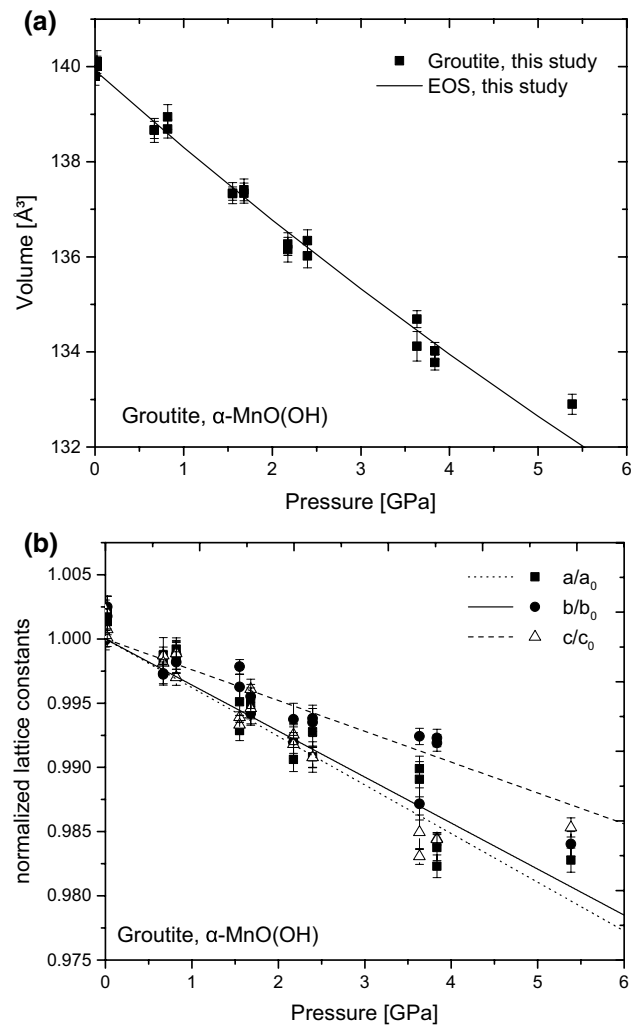| h k l	d_{obs}	d_{calc}	$d_{obs} - d_{calc}$
−1 1 1	3.332	3.346	−0.014
0 2 0	2.586	2.588	−0.002
1 1 1	2.485	2.491	−0.006
0 0 2	2.386	2.385	0.001
2 0 0	2.386	2.385	0.001
−1 2 1	2.226	2.229	−0.003
0 1 2	2.165	2.166	−0.001
2 1 0	2.165	2.166	−0.001
0 2 2	1.754	1.754	0.000
2 2 0	1.754	1.754	0.000
−1 1 3	1.646	1.646	0.000
−3 1 1	1.646	1.646	0.000
−1 3 1	1.606	1.605	0.001
1 3 1	1.475	1.475	0.000
2 0 2	1.421	1.421	0.000
2 2 2	1.245	1.245	0.000

Fig. 8 a Volume compressibility of groutite at room temperature, **b** Compressibility behavior of the cell parameters of groutite at room temperature normalized to values from Kohler et al. (1997). Linear fits are shown to guide the eye

Fig. 7 Proposed pressure–temperature diagram of the MnO(OH) system showing all measured points and postulated phase boundaries similar to the FeO(OH) system. The *shaded gray line* illustrates a low geothermal gradient (≈4.4°/km) under continental shields [after Jaupart and Mareschal (1999) and Winter (2014)] which is very similar to the cold Martian thermal gradient suggested by Verhoeven et al. (2005) and Zharkov and Gudkova (2014)

MnO(OH): equation of state

Unit-cell volume and unit-cell parameters of the MnO(OH) polymorphs as a function of pressure are shown in Figs. 8 and 9.

The MnO(OH) phases are more compressible than their Fe analogues. From a fit of Eq. (1) to the high-pressure data at room temperature, we obtained K(groutite) = (84.0 ± 2.9) GPa, V_0 = (139.92 ± 0.13) Å^3, (K' = 4) (cf. Fig. 8) and K(manganite) = (82.2 ± 3.0) GPa, V_0 = (135.37 ± 0.15) Å^3, (K' = 4) which is lower than the value reported by Suzuki (2013) (cf. Table 1). As can be seen in Fig. 9a, Suzuki's (2013) measurements agree well with our measurements up to 4 GPa. At higher pressure, they deviate significantly from our curve, perhaps indicating problems with non-hydrostaticity. The unusual high K' value 7 obtained by Suzuki (2013) points to the same direction.

Because the *P-T* space covered by our data is too limited, we did not derive the volumetric thermal expansion coefficient α for the MnO(OH) polymorphs from a fit to Eq. (1). Instead, α for both phases was obtained from the study of Kohler et al. (1997, their Table 4) by a linear approximation
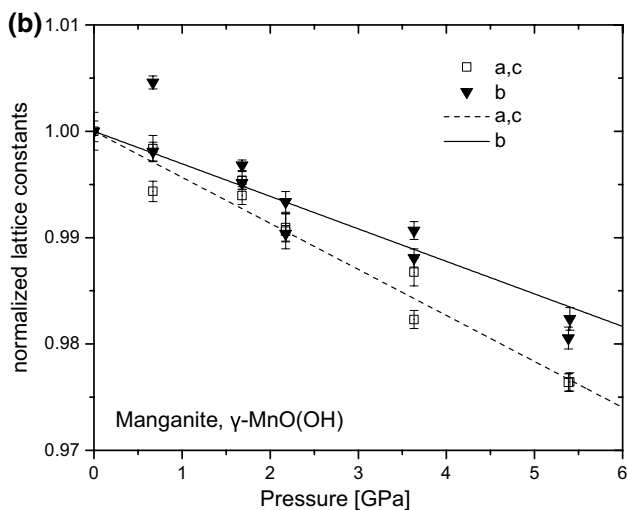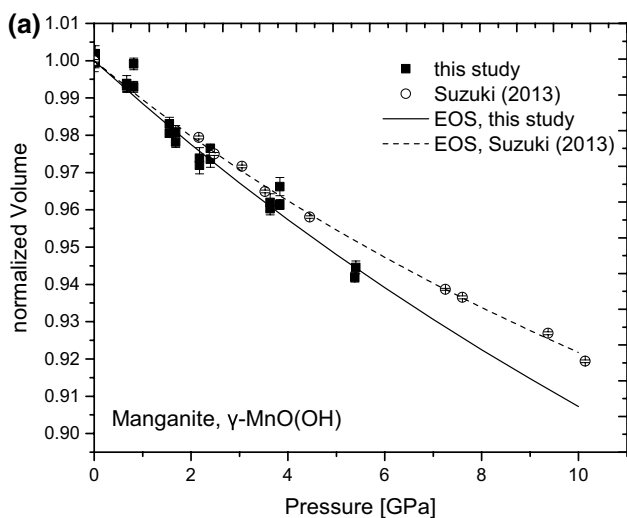
(a)

(b)

Fig. 9 a Volume compressibility of manganite at room temperature in comparison with the literature values normalized to values from Kohler et al. (1997). **b** Compressibility behavior of the cell parameters of manganite at room temperature in comparison with the literature values normalized to values from Kohler et al. (1997). Linear fits are shown to guide the eye

$$V_T = V_0\left(1 + \alpha\left(T - T_0\right)\right)^3 \qquad (3)$$

The results are almost identical, $\alpha(\text{groutite}) = 1.565 \times 10^{-5}$ K^{-1}, $\alpha(\text{manganite}) = 1.564 \times 10^{-5}$ K^{-1}. For manganite, this value can be compared to an estimate obtained from run 5. Figure 10 depicts the unit-cell volume of manganite (run 5–6 to run 5–14) as a function of temperature. $\alpha_{\text{run 5}}(\text{manganite}) = 1.597 \times 10^{-5}$ K^{-1}, which was calculated from the mean room temperature volumes (run 5–6, run 5–6b) and the value at $T = 450$ °C, is very similar to the value above.

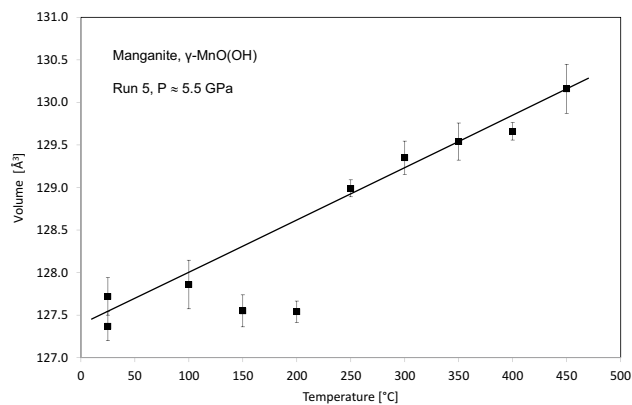**Fig. 10** Thermal expansion of manganite at $P \approx 5.5$ GPa (run 5). $\alpha_{\text{run 5}}(\text{manganite}) = 1.597 \times 10^{-5}$ K^{-1} was calculated from the mean room temperature volumes (run 5–6, run 5–6b) and the value at $T = 450$ °C. *Solid line* calculated volume (Eq. 3)

Conclusions

In this study, the bulk modulus of goethite was determined as (112.26 ± 2.26) GPa which is in very close agreement to the values provided by Nagai et al. (2003) and Fernando et al. (2012). Goethite is more compressible than its structural Al-analogue diaspore. The compressibility data reported by Kim and Yi (1997) and Gleason et al. (2008) seem to be too low probably caused by non-hydrostatic conditions in their experiments.

On the other hand, the thermal expansion coefficient of goethite is not sufficiently constrained yet. The value obtained in this study $\alpha = (4.97 \pm 1.03) \times 10^{-5}$ K^{-1} is significantly higher than the value given by Gleason et al. (2008), $\alpha = (2.3 \pm 0.6) \times 10^{-5}$ K^{-1}. Further investigations are needed at this point.

Majzlan et al. (2003b) generated an internally consistent thermodynamic data set for goethite and hematite by mathematical programming analysis (MAP). This method combines calorimetric measurements on one hand and phase-equilibrium bracketing experiments on the other hand. They provided two slightly different datasets (Table 5 in Majzlan et al. 2003b) based on the phase-equilibria data of Baneyeva and Bendeliani (1973) and Voigt and Will (1981), respectively. The reaction boundaries for the dehydration of goethite and for the phase transition between α-FeO(OH) and ε-FeO(OH) have been further constrained by the data presented in this study. The stability fields proposed by Voigt and Will (1981) are confirmed within uncertainties. Therefore, we recommend the use of the standard thermodynamic data for goethite derived from the Voigt and Will (1981) brackets: $\Delta H^0_{\text{f}}(\text{goethite}) = -561.4$ kJ mol^{-1}, and S^0 (goethite) $= 59.5$ J K^{-1} mol^{-1}.

This study shows evidence for similarities in the pressure–temperature phase diagrams for FeO(OH) and

MnO(OH) (Figs. 2, 7). Like the α-FeO(OH)–ε-FeO(OH) phase transition, we propose a high-pressure phase transition α-MnO(OH) (groutite)–γ-MnO(OH) (manganite). The dehydration temperature of MnO(OH) was constrained as well. The shaded gray line shown in Figs. 2 and 7 illustrates a low geothermal gradient (approx. 4.4°/km) under stable continental crust (cratons) [after Jaupart and Mareschal (1999) and Winter (2014)] which is very similar to the cold Martian thermal gradient suggested by Verhoeven et al. (2005) and Zharkov and Gudkova (2014). Since hotter profiles are much shallower, P-T conditions of the phase transitions α-FeO(OH)–ε-FeO(OH) and α-MnO(OH)–γ-MnO(OH) are probably not realized on Earth or terrestrial planets.

Additionally, first compressibility data for groutite and further P-V-T data for manganite could be presented.

References

Baneyeva MI, Bendeliani NA (1973) The Fe_2O_3-H_2O system at high pressures and extemperatures. Geochem Int 10:840–842

Bendeliani NA, Baneyeva MI, Poryvkin DS (1972) Synthesis of new modification of FeO(OH), stable at high pressure. Geochem Int 9:589–590

Chabre Y, Pannetier J (1995) Structural and electrochemical properties of the proton/γ-MnO_2 system. Prog Solid State Chem 23:1–130

Chenavas J, Joubert JC, Capponi JJ, Marezio M (1973) Synthese de nouvelles phases denses d'oxyhydroxydes $M^{3+}OOH$ des metaux de la premiere serie de transition, en milieu hydrothermal à tres haute pression. J Solid State Chem 6:1–15

Chukhrov FV, Gorshkov AI, Sivtsov AV, Berezovskaya VV, Dikov YP, Dubinina GA, Varinov NN (1989) Akhtenskite—the natural analog of ε-MnO_2. Int Geol Rev 31:1068–1072

Darul J, Lathe C, Piszora P (2013) Mn_3O_4 under high pressure and temperature: thermal stability, polymorphism, and elastic properties. J Phys Chem C 117:23487–23494

Decker DL (1971) High-pressure equation of state for NaCl, KCl, and CsCl. J Appl Phys 42:3239–3244

Fernando S, Baynes M, Chen B, Banfield JF, Zhang H (2012) Compressibility and structural stability of nanoparticulate goethite. RSC Adv 2:6768–6772

Gleason AE, Jeanloz R, Kunz M (2008) Pressure-temperature stability studies of FeOOH using X-ray diffraction. Am Mineral 93:1882–1885

Grevel K-D, Burchard M, Faßhauer DW, Peun T (2000) Pressure-volume-temperature behavior of diaspore and corundum: an in situ X-ray diffraction study comparing different pressure media. J Geophys Res 105(B12):27877–27887

Gruner JW (1947) Groutite, $HMnO_2$, a new mineral of the diaspore-goethite group. Am Mineral 32:654–659

Gualtieri AF, Venturelli P (1999) In situ study of the goethite-hematite phase transformation by real time synchrotron powder diffraction. Am Mineral 84:895–904

Jaupart C, Mareschal JC (1999) The thermal structure and thickness of continental roots. Lithos 48:93–114

Kim Y-H, Yi Z (1997) High pressure X-ray diffraction study on a goethite using synchrotron radiation. J Mineral Soc Korea 10:75–81

Klein C, Hurlbut Jr CS (1993) Manual of mineralogy, 21st edn. Wiley p 394

Klingsberg C, Roy R (1959) Stability and interconvertibility of phases in the system Mn-O-OH. Am Mineral 44:819–838

Kohler T, Armbruster T, Libowitzky E (1997) Hydrogen bonding and Jahn–Teller distortion in groutite, α-MnOOH, and manganite, γ-MnOOH, and their relations to the manganese dioxides ramsdellite and pyrolusite. J Solid State Chem 133:486–500

Lauterjung J, Will G, Hinze E (1985) A fully automatic peak-search program for the evaluation of Gauss-shaped diffraction patterns. Nucl Inst Meth Phys Res A 239:281–287

Majzlan J, Lang BE, Stevens R, Navrotsky A, Woodfield BF, Boerio-Goates J (2003a) Thermodynamics of Fe oxides: Part I. Entropy at standard temperature and pressure and heat capacity of goethite (α-FeOOH), lepidocrocite (γ-FeOOH), and maghemite (γ-Fe_2O_3). Am Mineral 88:846–854

Majzlan J, Grevel K-D, Navrotsky A (2003b) Thermodynamics of Fe oxides: Part II. Enthalpies of formation and relative stability of goethite (α-FeOOH), lepidocrocite (γ-FeOOH), and maghemite (γ-Fe_2O_3). Am Mineral 88:855–859

Majzlan J, Brey-Funke M, Malz A, Donndorf S, Milovský R (2016) Fluid evolution and mineralogy of Mn-Fe-barite-fluorite mineralizations at the contact of the Thuringian Basin, Thüringer Wald and Thüringer Schiefergebirge in Germany. Geol Carphat 67(1):3–20

Nagai T, Kagi H, Yamanaka T (2003) Variation of hydrogen bonded O-O distances in goethite at high pressure. Am Mineral 88:1423–1427

Paris E, Ross CR II, Olijnyk H (1992) Mn_3O_4 at high pressure: a diamond-anvil cell study and a structural modelling. Eur J Mineral 4:87–93

Post JE, Heaney PJ (2004) Neutron and synchrotron X-ray diffraction study of the structures and dehydration behaviors of ramsdellite and "groutellite". Am Mineral 89:969–975

Rask JH, Buseck PR (1986) Topotactic relations among pyrolusite, manganite, and Mn_5O_8: a high-resolution transmission electron microscopy investigation. Am Mineral 71:805–814

Reid AF, Ringwood AE (1969) Newly observed high pressure transformations in Mn_3O_4, $CaAl_2O_4$, and $ZrSiO_4$. Earth Planet Sci Lett 6:205–208

Ross CR, Rubie DC, Paris E (1990) Rietveld refinement of the high-pressure polymorph of Mn_3O_4. Am Mineral 75:1249–1252

Suzuki A (2010) High-pressure X-ray diffraction study of ε-FeOOH. Phys Chem Minerals 37:153–157

Suzuki A (2013) Compression behaviour of manganite. J Mineral Petrol Sci 108:295–299

Verhoeven O, Rivoldini A, Vacher P, Mocquet A, Choblet G, Menvielle M, Dehant V, Van Hoolst T, Sleewaegen J, Barriot J-P, Lognonne P (2005) Interior structure of terrestrial planets: Modeling Mars' mantle and its electromagnetic, geodetic, and seismic properties. J Geophys Res 110:E04009. doi:10.1029/2004JE002271

Voigt R, Will G (1981) Das System Fe_2O_3-H_2O unter hohen Drücken (The system Fe_2O_3-H_2O under high pressures). N Jb Mineral Mh (2):89–96

Winter JD (2014) Principles of igneous and metamorphic petrology, 2nd edn. Pearson Education Limited, Harlow, Essex CM20 2JE, England, 738 + IV p

Zharkov VN, Gudkova TV (2014) Seismic model of Mars: Effects of hydration. Planet Space Sci 104:270–278